




Phase diagram and deuteration contribution to the phonon analysis of the normal-to-incommensurate phase transition of 4-4' dichlorobiphenyl sulfone determined using Raman and neutron scattering

M. Sougati ^{1,2,*}, F. Le Marrec,^{1,3} S. Beaufils,¹ J. Ollivier,⁴ P. Bourges,⁵ B. Toudic ^{1,†} and C. Ecolivet ^{1,‡}

¹Université de Rennes, CNRS, IPR (Institut de Physique de Rennes)-UMR 6251, F-35000 Rennes, France

²Département de Physique, Laboratoire de Physique et de Chimie de l'Environnement, Université Joseph KI-ZERBO (ex Université de Ouagadougou), 03 BP 7021 Ouagadougou 03, Burkina Faso

³Laboratoire de Physique de la Matière Condensée, Université de Picardie Jules Verne, 33 rue Saint Leu, 80039 Amiens Cedex 1, France

⁴Institut Laue-Langevin, 71 Avenue des Martyrs, 38000 Grenoble, France

⁵Université Paris-Saclay, CNRS, CEA, Laboratoire Léon Brillouin, 91191 Gif-sur-Yvette, France



(Received 5 April 2024; revised 24 May 2024; accepted 14 June 2024; published 1 July 2024)

4-4'-dichlorobiphenyl sulfone (BCPS) presents a phase transition from a high-symmetry monoclinic phase $I2/a$ to an incommensurate phase $I2/a$ ($0\beta 0$) at $T_i = 150$ K without any lock-in phase transition observed down to the lowest temperatures at atmospheric pressure. Such examples which remain incommensurate close to 0 K are quite rare and are prototype materials for the study of the competitive terms between internal energy and residual entropic contributions defining their stable phases. The present study reports an experimental determination of the temperature versus pressure phase diagram for BCPS. A Raman study of the amplitudon mode in the incommensurate phase reveals that the transition temperature diminishes under pressure and vanishes at about 320 MPa for the hydrogenated compound. It also sheds light on the properties of the low-frequency phonons and their assignments by a hydrogen isotopes comparison. In particular, it shows that the chlorophenyl torsion modes have frequencies in the 100 cm^{-1} range and cannot be a primary order parameter. A neutron-diffraction experiment reveals that there is no tendency for a lock-in phase transition at any pressure, with the critical wave vector remaining always far away from any simple rational value. Inelastic neutron-scattering experiments on the deuterated compound versus pressure at 50 K report, as expected, much lower damping of the critical excitations around T_i compared to the ones at atmospheric pressure ($T_i = 150$ K). It reveals the complexity of the spectral function when both soft mode and central peak are present and allows the observation of both the phason and the amplitudon modes at lower pressure within the incommensurate phase. High-resolution neutron diffraction carried out at the same temperature reveals very different pressure responses of the crystallographic parameters inducing deviatoric strains.

DOI: [10.1103/PhysRevB.110.024103](https://doi.org/10.1103/PhysRevB.110.024103)

I. INTRODUCTION

Among the aperiodic crystals—incommensurate modulated, aperiodic composites, and quasicrystals—the more extensively studied ones with the best understanding are undoubtedly the modulated phases [1–5]. Being usually located between a high-symmetry prototype phase and a lock-in phase, they allow an easier perturbative approach in relation to the second-order phase transition occurring at T_i between the prototype and the incommensurate phase. In order to model such structures, the knowledge of the lock-in phase structure is a powerful advantage. Usually, the variation of the modulation vector \mathbf{q}_s moving toward a simple commensurate value can also indicate a final more stable structure. Very rarely, the incommensurate phase remains at the lowest temperatures [6] but the 4,4'-dichlorophenyl sulfone ($\text{ClC}_6\text{H}_4)_2\text{SO}_2$,

abbreviated later on as BCPS, is such an exception [7–12]. In fact, a small temperature variation of \mathbf{q}_s is observed from $0.775\mathbf{b}^*$ at $T_i = 150$ K to $0.787\mathbf{b}^*$ at 15 K, which does not seem to be closer to any low dimensionality ratio [10].

This crystal has a monoclinic structure with an antiferro ordering along a direction close to \mathbf{a} as shown in Fig. 1, but it is often described using a more convenient centered cell closer to an orthorhombic one: $I2/a$, $Z = 4$, $a = 20.22 \text{ \AA}$, $b = 5.00 \text{ \AA}$, $c = 12.25 \text{ \AA}$, and $\beta = 90.57^\circ$ [11]. The other molecules of the nonprimitive cell are obtained by applying the inversion $\{I|\frac{1}{2}\frac{1}{2}\frac{1}{2}\}$. Among the peculiarities of this compound, we may notice first, the negative thermal expansion along \mathbf{a} [10] and, secondly, the unusually small damping of the soft mode at the origin of this structural phase transition (SPT) [13] similar to calomel [14] or chloranil [15] examples. Crystals that remain aperiodic down to the lowest temperatures, like BCPS at atmospheric pressure, are prototype compounds for the study of structural phases with residual entropy contributions. Their specific very low-energy collective excitations, the phason branches, remain indeed present around 0 K in addition to the usual Goldstone modes, the acoustic phonon branches.

*Contact author: msougoti@gmail.com

†Contact author: bertrand.toudic@univ-rennes.fr

‡Contact author: claude.ecolivet@univ-rennes.fr

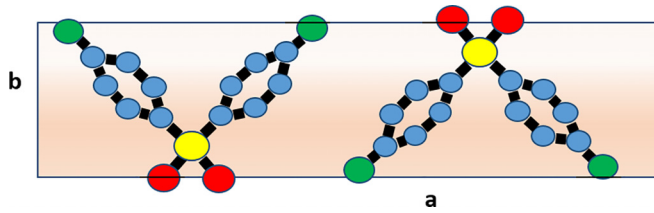


FIG. 1. Schematic view of the BCPS structure along the **a** direction using the primitive cell representation with two molecules per cell. Yellow and green refer to sulfur and chlorine atoms, respectively, red to oxygen, and blue to carbon. The hydrogen atoms bonded to carbons are not shown.

Very low-temperature specific heat C_p behavior in BCPS is indeed attributed to these modes in the millikelvin range at atmospheric pressure [16,17]. Other techniques such as nuclear resonance techniques also probe these very slow dynamical fluctuations and were applied in BCPS at low temperatures [12,18,19].

Very detailed complementary observations of the collective critical dynamics are obtained by Raman and neutron scattering. Coherent neutron scattering has revealed specific features of this displacive incommensurate phase transition at atmospheric pressure studying them from both sides of the transition temperature T_i at ambient pressure [13]. A frequency gap is observed for the high-symmetry soft mode and for the apparent amplitudon and phason modes just above and below the temperature T_i , respectively. However, as expected for displacive phase transitions around a second-order phase transition, the integral of a whole scattering spectrum diverges following the temperature dependence of the static susceptibility [13]. This is explained by the appearance of the so-called central peak to which the intensity is transferred [20,21]. This central peak has a resolved width in the reciprocal space, which means finite correlation lengths in the real space, but this central peak is not resolved in energy using coherent neutron scattering. Like in an ordinary phase transition, in the low-temperature phase, the soft mode, here the amplitudon, is totally symmetric and henceforth always Raman active. Due to the rather small value of the gap ($<3 \text{ cm}^{-1}$) for conventional grating spectrometers, observations were carried out using a triple-pass tandem of Fabry-Perot interferometers [22]. With the benefit of high contrast and a resolution of 0.1 cm^{-1} , it revealed in-phase and antiphase scattering coupling between the amplitudon and longitudinal acoustic modes as well as an apparent saturation of this mode frequency 3 K below T_i . This was also observed by coherent inelastic neutron-scattering measurements, which also revealed the phason mode with a gap below T_i and a central peak in addition to soft modes in both phases [13]. Despite such clear observations and the identification of the atomic displacements generated by the incommensurate modulation [11], the identification of the antagonist interactions and their formulation at the level of molecular motions driving this incommensurate SPT is still an ongoing challenge. The role of the phenyl rings in this SPT was a long time in debate, due to the resemblance borne by the BCPS molecule with biphenyl [23,24]. Then lattice dynamics studies, first on the basis of atom-atom potentials in rigid molecules [25,26] and later with

ab initio computations of internal vibrations [27], have found that the torsion modes of phenyl rings were located at higher frequencies where the coupling to the soft mode would require a huge dispersion of these modes. All these lattice dynamics studies find frequency dips close to $\mathbf{q}_s = 0.78\mathbf{b}^*$ in the lowest phonon transverse acoustic dispersion branch. However, they do not depend on the internal molecular rigidity and are even found in the bromide compound that does not undergo such a phase transition. They have also shown that these frequency dips involve a complex polarization, in rather good agreement with the modulations determined by x-ray diffraction [11] making difficult the formulation of a simple mechanism that could steer this SPT. A molecular dynamics study has also described the anomalous expansion anomaly and the existence of an incommensurate phase transition [28] with results similar to the experimental ones. Nevertheless, to our best knowledge, no published experimental data directly clears the phenyl torsions of the main role in this transition. In order to find an experimental answer, we report light-scattering experiments on deuterated crystals. In the absence of strong hydrogen bonding, this single substitution of hydrogen by deuterium atoms should only alter the molecular inertia moments avoiding strong variations of interatomic force fields that occur, e.g., with halogen exchange [29]. Such a study could have identified the phenyl torsion modes unaffected by this modification, but unfortunately a simultaneous deuterium substitution mixed the different effects precluding the identification of phenyl torsions. In our simpler substitution, more than other low-frequency modes, phenyl torsion should present the stronger frequency variations by taking advantage of the distance of the four hydrogen atoms to each S-Cl torsion axis. This study is also an opportunity for a detailed analysis of the temperature behavior of all modes observed in the lattice modes range in the incommensurate phase and above, since anomalous temperature variations of frequencies, linewidths, or intensities are interesting clues for a better understanding of this incommensurate phase.

Thus far, all the studies concerning this phase transition were performed at atmospheric pressure. In organic crystals, where usually van der Waals interactions dominate, a moderate pressure of a few hundred megapascal is sufficient to produce measurable effects. It provides a unique opportunity to continuously modify the interactions balance. The phase diagram (T,P) gives direct information on the relative intramolecular and intermolecular forces. This gives a unique opportunity to study the critical pretransitional phenomena around an incommensurate phase transition on approaching the so-called displacive limit of a displacive phase transition [30]. Complementary light- and neutron-scattering investigations offer a wider scope by their ability to study structural and dynamical aspects, giving access to the high-temperature phase soft mode and to both soft excitations, namely, the phason and the amplitudon in deuterated crystals at different pressures and temperatures.

II. EXPERIMENT

BCPS crystals, both deuterated and hydrogenated, were grown by a Bridgman method giving after multiple crystallizations, good quality crystals with excellent (**b,c**) cleavage

planes as previously reported [22]. Deuterated specimens grown by the same method present an isotopic exchange above 99%. Large slab samples (**a***,**b**,**c**) have been used in this study, even if the principal optical axes inside the (**a**,**c**) planes are at 17° from the crystallographic directions [31]. Consequently, Raman spectra involving light polarized along **a*** and **c** present polarization leaks. Moreover, noticing that the monoclinic angle deviates only from a fraction of a degree, we will not differentiate the **a** and **a*** directions in the following.

Raman experiments used the green line of an argon ion laser working at 514.5 nm and a triple grating spectrometer (DILOR Z24) with a resolution of 0.8 cm^{-1} . Recorded spectra are analyzed by fitting to damped oscillator profiles convoluted with the instrumental resolution. Low-temperature experiments used an atmosphere of cooled He or nitrogen gases with a three-term temperature regulation giving a stability better than 0.1 K, whereas the absolute temperature uncertainty is about 0.5 K. A high-pressure cell working up to 400 MPa previously described [32] was inserted in this cryogenic set for stable pressure and temperature conditions.

Neutron experiments were performed at the Laboratoire Léon Brillouin in Saclay using the triple-axis spectrometer 4F1 installed on a cold neutron source. Such an instrument offers both a very high energy and spatial resolutions, as required here. The incident wave vector is $k_i = 1.20 \text{ \AA}^{-1}$, which gives an incoherent elastic energy resolution of 20 GHz ($\sim 80 \text{ \mu eV}$) full width at half maximum measured on a vanadium specimen. A beryllium filter was used to avoid contamination of higher-order harmonics in the incident neutron beam and no collimation was used during the experiments. The spatial resolution was $\Delta Q < 10^{-2} \text{ \AA}^{-1}$ as measured at a satellite Bragg position. A helium gas pressure cell was used up to 0.5 GPa, possibly cooled down to 4 K. A single crystal of fully deuterated $(\text{ClC}_6\text{D}_4)_2\text{SO}_2$ of 0.25 mm^3 was studied. Its mosaicity was measured of the order of 1.6° . The crystal was mounted with the (**a**,**b**) plane in the horizontal scattering plane of the triple-axis spectrometer, so only the reciprocal vectors within the (**a***,**b***) plane were accessible.

III. RAMAN STUDY AT ROOM TEMPERATURE AND ATMOSPHERIC PRESSURE

A. Phonons assignment

As reported in literature [23], the six Raman-active lattice modes ($2A_g + 4B_g$) predicted by group theory do not allow an assignment of all the observed Raman lines; there must be at least three internal modes ($2A_g + 1B_g$) in this frequency range. These internal modes are assigned in the literature on the one hand as a bending or “butterfly” A_g mode labeled α here and, on the other hand, as symmetric and antisymmetric chlorophenyl torsions labeled φ^+ and φ^- . Spectra with all possible polarizations were previously reported at room temperature [23] and only two polarizations allow a full view of all these modes: (**a**,**a**) for the A_g ones and (**b**,**c**) for the B_g ones with the maximum intensity for the highest frequency modes. Consequently, Figs. 2(a) and 2(b) display Raman spectra of hydrogenated and deuterated BCPS recorded in the **c(a,a)b** and the **c(b,c)a** configuration in the Porto notation. Polarization leakage from the intense A_g modes **2**, **5**, and **7**

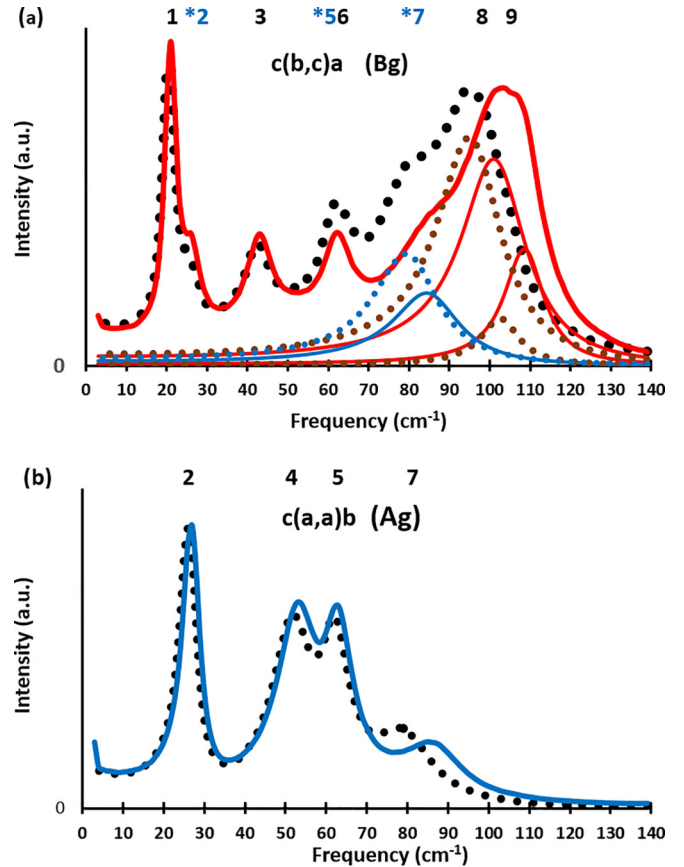


FIG. 2. Room-temperature low-frequency Raman lines for the hydrogenated crystal with continuous lines and deuterated crystals with dotted lines. Blue refers to the A_g symmetry and red to the B_g symmetry. In (a) the **c(b,c)a** spectrum shows the B_g symmetry modes (**1,3,6,8**, and **9**) and three A_g ones (**2, 5**, and **7**) via a (**c,c**) polarization leakage indicated by a star. Mode **7** appears with thin blue lines in the decomposition. In the 100 cm^{-1} (3 THz) range, the decomposition of the **8** and **9** modes appears in red with the same code as for **7**. In (b) the **c(a,a)b** spectrum shows the A_g modes (**2, 4, 5**, and **7**). Since all fit lines coincide with the spectra in this frequency range at a few percent, the fitted lines are not shown for clarity.

in the (**c,c**) polarization allows also their observation in the (**b,c**) spectrum. The narrow line **2** nearly superposes on the **1** whereas **5** and **6** are undistinguishable. The broader line **7** builds a block with the **8** and **9** and they only appear via a fit. From these spectra and the results of which are gathered in Table I, the effect of deuteration is obviously larger on the unresolved block of the **7**, **8**, and **9** modes than on the other low-frequency modes. The best way to quantify this effect is the ratio of the frequencies of the same modes for both isotopes (ν_H/ν_D). It can be compared to the square root of the masses or the inertial moments ratio involved in the motion. In the present case, hydrogen atoms count for less than 3% of the molecular weight; the relative frequency ratio between the isotopes for translational modes should not be greater than 1.014. A similar value is obtained for libration frequencies due to the inertial rotation moments around the longest and shortest molecular axes and a somewhat smaller value of 1.01 around the median axis. However, the location of the

TABLE I. Room-temperature frequencies, linewidths (in cm^{-1}), and symmetries of the Raman lines of the hydrogenated (H) and deuterated (D) BCPS. The absolute calibration of frequencies is better than 0.5 cm^{-1} , whereas the reproducibility of spectra is about 0.2 cm^{-1} but could be larger for the unresolved modes. The lowest lines indicate the main component of each mode polarization and the mode frequency as in [27].

Modes	1	2	3	4	5	6	7	8	9
H (cm^{-1})	21.1	26.7	43.4	53.1	62.2	62.8	86.0	102.6	109.2
D (cm^{-1})	20.6	26.1	42.9	51.2	62.0	62.4	79.8	96.8	103.2
$\nu_{\text{H}}/\nu_{\text{D}}$	1.02	1.02	1.01	1.04	1.00	1.01	1.08	1.06	1.06
FWHM (cm^{-1})	3.0	5.5	8.5	10.5	10.0	9.0	19.5	20.0	12.0
Symmetry	Bg	Ag	Bg	Ag	Ag	Bg	Ag	Bg	Bg
Ref. [22]	T_x	T_y	R_z	α	R_y	R_x	$\varphi-$	T_z	$\varphi+$
Freq. (cm^{-1})	17	26	45	40	57	52	81	66	95

inversion center between the molecules does not allow sorting out translations from librations. Then, the isotopic frequency ratio should belong to the 1.01–1.02 range as shown in Table I. This is the case of the modes **1**, **2**, **3**, **5**, and **6** whereas the **4** mode is slightly above. Among the low-frequency internal modes, the maximum effect is expected for chlorophenyl torsions.

By comparing the deuterated and hydrogenated phenyl rings inertial moments with respect to the S-Cl axis, a ratio of 1.097 should be observed between the frequencies of both phenyl torsion modes. According to the fits shown in Fig. 2 and from other polarizations, it appears that this ratio for the Ag **7** mode with 1.08 is very close to this value. Obtaining its value for the **8** and **9** Bg modes requires a decomposition at room temperature for the (**b,c**) polarization which gives about 1.06 for each mode using a least-square method. Similar values are also found with the (**b,a**) polarization, where this high-frequency block presents more even contributions of these modes. Although the total relative shift of these modes (2.12) is in reasonable agreement with the expected one (2.11), the assignment of these two Bg modes remains unsolved. However, in this computed ratio we suppose that the observed modes are harmonic without any perturbation of the force constant due to isotopic exchange, whereas the observed Raman lines present a significant damping of anharmonic origin. In fact, the temperature evolution of the **8** mode's frequency presents a smaller increase on cooling for the deuterated crystal resulting in a ratio of 1.015 at 90 K whereas its damping is halved. This observation suggests that this mode is very likely a lattice mode and the **9** mode a chlorophenyl torsion one [26,27]. Nevertheless, this mode presents a similar temperature behavior in both crystals keeping the same poor agreement (1.05). However, lattice dynamics studies are also a bit deceiving in the description of the **8** mode since the relative discrepancies between the computed and the experimental frequencies reach one-third for the more recent one using *ab initio* calculations for the internal modes [27] and one-fourth for the former one [26]. This slightly better result could be related to a greater coupling of internal and external mode polarizations appearing in Table 2 in Ref. [29] suggesting a possibly more complex polarization of modes **8** and **9**. As for the chlorophenyl bending mode, the frequency ratio of 1.04 for the **4** suggests an intramolecular origin for this Bg mode. Despite a rather poor frequency agreement with the *ab initio* calculations (30%) it could be assigned to the α (Ag)

mode at 40 cm^{-1} . By using several scattering configurations, which modify the relative intensities in the spectra, it was possible to obtain with good accuracy the frequency and the linewidths of all these modes at room temperature. They are presented in Table I, both for hydrogenated and deuterated BCPS. This table gathers the isotopic frequencies and their ratio for all the Raman frequencies observed below 140 cm^{-1} and their symmetry at room temperature. It also allows a comparison with the more recent dynamical calculations [27] of the expected frequency and the main polarization of each mode. The linewidths, unreported up to now, reveal an increase roughly proportional to the mode frequency with the greater damping for the **7** and **8** modes.

B. Incommensurate features

Apart from the presence of a soft mode, signatures of the incommensurate phase transition in this compound are rather weak, identified only by small kinks in the temperature evolution of mode frequencies. This kind of anomalies usually results from a biquadratic coupling between the order parameter and a phonon, but in this compound where the temperature behavior of the order parameter is close to $(T_i - T)^{1/2}$, it may also result from a linear coupling of the phonon with the square of the order parameter.

These anomalies were first observed and studied down to the lowest temperatures on hydrogenated BCPS single crystals [23], and later confirmed by a powder study [29]. However, nothing was reported about the anharmonicity in this compound observable through the linewidths evolution. In order to get a deeper understanding of the dynamics of this incommensurate compound, we also undertook a quantitative determination of the intensity evolution. We restrict this analysis to the 80–300 K range for the lower-frequency modes appearing in the Ag: **c(b,b)a** configuration where the soft mode is the most intense and without any strong contribution from the broader **7**, **8**, and **9** modes studied in the above paragraph. A comparison with the room-temperature spectrum is possible in Ref. [23]. This configuration allows also a better study of the Raman modes activated in the incommensurate phase. A typical Ag spectrum of the nondeuterated crystal recorded at $T = 93 \text{ K}$ appears as the solid blue line in Fig. 3. Raman lines of the normal phase below 150 K are labeled by the same numbers, whereas the modes activated by the incommensurate modulation are labeled by the same letters as

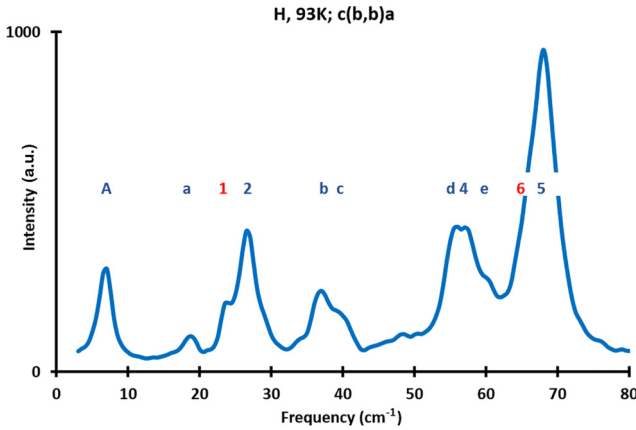


FIG. 3. Low-temperature (93 K) **c(b,b)a** Raman spectrum for hydrogenated BCPS. The hard modes already present at high temperatures are labeled like in Fig. 2 whereas the more intense lines appearing in the incommensurate phase are labeled by letters from a to e in addition to the amplitudon (A). Bg modes **1** and unresolved **6** appear via a **(b,a)** polarization leakage.

in the former single-crystal study [23]. As already observed, mode **5** has at low temperatures a higher frequency than mode **6** and also a greater intensity which may partially mask it. A similar temperature evolution of the deuterated crystal spectra is observed in this frequency range.

C. Raman intensities

Although polarized spectra at different temperatures are also reported in Ref. [23], there is still some interest to make a quantitative study of the mode intensities, and in particular for those activated by incommensurability. Like in any nonferroic normal SPT, the origin of the Raman lines induced in the low-temperature phase may be understood by a Brillouin zone folding of the phonon dispersion branches. Due to the incommensurability of the critical wave vector $\pm\mathbf{q}_s$, an infinity of zone folding occurs at different discrete locations defined by $\mathbf{G} \pm n \cdot \mathbf{q}_s$, n being an integer and \mathbf{G} a reciprocal lattice vector. To some extent, all these phonons activated by incommensurability generate a p th-order Raman scattering involving $(p-1)$ phonons at \mathbf{q}_s [33]. Then, phonon pseudo-momentum conservation requires that $(p-1)\mathbf{q}_s + \mathbf{q} + \mathbf{G} = \mathbf{k}_s - \mathbf{k}_i$, where \mathbf{q} is the phonon wave vector and $\mathbf{k}_s - \mathbf{k}_i$ is the transfer wave vector of the scattered photon. The efficiency of this multiphonon process is governed by the product of the order parameter by the population of the phonons involved in this process. These parameters vary in opposite directions versus temperature; the phonon population decreases with decreasing temperatures whereas the order parameter increases. For a Stokes process (phonon creation), their Raman intensity should then vary like $[n(h\nu/k_B T) + 1](T_i - T)^{2\beta(p-1)}$, where β is the order parameter exponent equal here to $\frac{1}{2}$ and $n(h\nu/k_B T)$ the phonon Bose factor. By studying the temperature evolution of the intensity of these Raman lines, it is possible to determine the order of the Raman process leading to the location of the observed phonons inside the Brillouin zone. Due to the infinite folding of branches, a broad weak Raman background appears where peaks occur for low-order processes and/or for higher

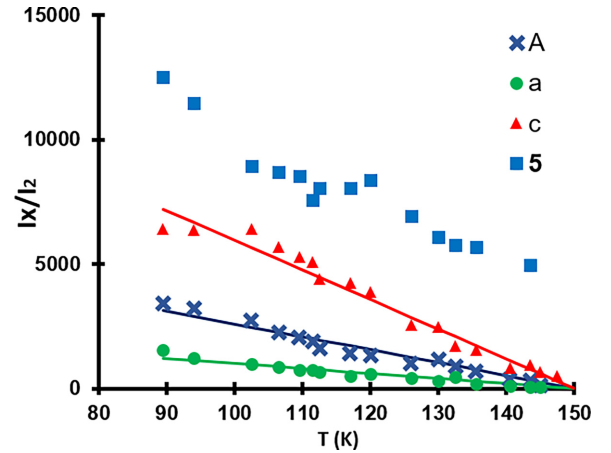


FIG. 4. Variation of the normalized intensities of some lines appearing in the incommensurate phase and of the hard mode 5 for comparison. Lines are guides to the eye.

density of states whereas holes in the spectrum are located in forbidden phonon bands. Figure 3 shows such contributions with a broad bump between 10 and 80 cm^{-1} for Bg modes that cannot be assigned simply to hard modes anharmonicity. Additional Raman lines activated by incommensurability appear rather close to the modes already observed with the same polarizations. The integrated intensities of these modes are normalized to the intensity of the standard mode **2**, seemingly unaffected by the transition, which varies only like the Bose factor. As shown in Fig. 4, in the temperature range 90–150 K, all lines present a linear variation vanishing at 150 K, indicating that $p = 2$. It means that these modes originate from $\pm\mathbf{q}_s$. The other lines previously reported appearing at lower temperature are likely the result of higher Raman-scattering orders generating power-law variations vs temperature corresponding to \mathbf{q}_s multiples ($p = 3$ mostly).

D. Hard mode linewidths

Figure 5 shows that most of the hard modes exhibit a normal anharmonicity regime with an increase of their linewidth with temperature. Aside from this usual behavior, we observe an anomalous behavior in the high-temperature phase of lines **1** and **3**, which both belong to the Bg symmetry and are assigned mainly to translations along **a**, and rotations around the **c** axis, respectively [27]. Strikingly, their linewidth evolution mimics the anomalous negative thermal expansion of the **a** lattice parameter, which is smaller in absolute value above than below T_i , and then very sensitive to the modifications of the long molecular axis. The origin of these behaviors lies mainly in the third-order anharmonicity, which contributes both to the thermal expansion and the phonons lifetime. At variance, the behavior of the Ag mode **5** presents a slight decrease of its linewidth on increasing temperature below T_i followed by the normal increase at higher temperatures. Such a low-temperature behavior is typical of a heterogeneous broadening where several unresolved modes contribute to the linewidth. Since it has a very close frequency to the Bg mode **6**, an artifact due to polarization leaks of these overlapping modes might be possible, but a contribution of

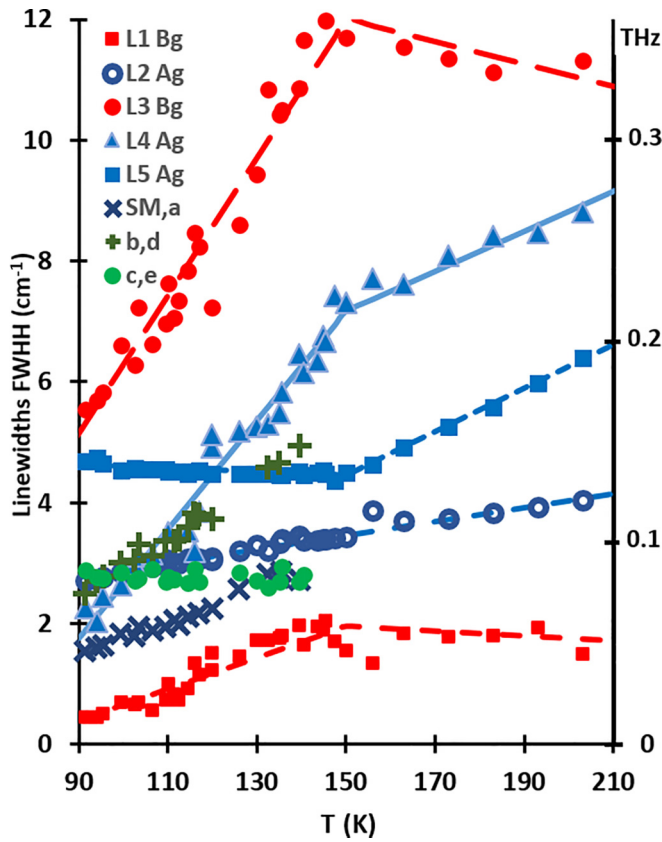


FIG. 5. Temperature evolution of the linewidths of hard modes and incommensurately activated modes. Lines are guides to the eye fitted to continuous kinks at $T_i = 150$ K. Hard Bg (Ag) modes are in red (blue). According to [27], dots and circles refer to modes with a larger amount of translations and squares to a larger amount of rotations, whereas triangles refer to the “butterfly” mode. Below T_i , black and green symbols show the linewidths evolution of the Raman lines activated by incommensurability as indicated in the legend.

incommensurate activated modes would also agree with the previous Raman study on single crystals [23]. The remaining Ag modes show a linewidth increase in both phases; a change of slope is observed for the butterfly mode **4**, but line **2** is perfectly continuous without any anomaly at T_i . This line, which also presents a perfectly monotonous frequency variation [23,29], is assigned mainly to translations along **b** with some contribution of the librations around the same axis. It is mostly unaffected by the phase transition since none of these displacements take part in the fundamental structural modulation [11,13]. In the incommensurate phase, the anharmonicity decreases under both cooling and ordering effects. Meanwhile, the Ag lines related either to motions along or around the **b** axis, or to the butterfly mode, exhibit a different but constant increase in both phases. Although these modes show different linewidths, neither of them is overdamped as in an order-disorder regime. In addition to the soft mode, some other lines (modes labeled *a*, *b*, *c*, *d*, *e* in Fig. 3) can also be resolved below T_i . These linewidths present similar behaviors to those of the hard modes, with the *c* and *e* Raman lines keeping the same value in this whole temperature range, whereas the other ones have a usual positive slope. However, it

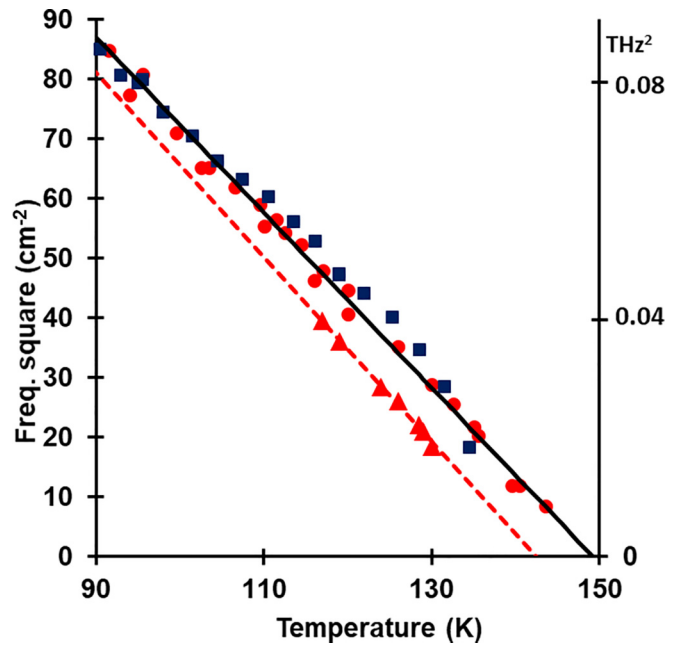


FIG. 6. Temperature evolution of the amplitudon frequency square in deuterated (■) and hydrogenated (●) BCPS at atmospheric pressure and at 60 MPa (▲) where lines are linear fits.

is noteworthy that they evolve by pairs: *a* with the soft mode and *b* with *d*, whereas *c* and *e* do not vary. It is tempting to assign these pairs to three distinct dispersion branches related to the hard modes in the neighborhood of \mathbf{q}_s .

E. Amplitudons

Figure 6 displays the amplitudon frequency square vs temperature for both compounds and it is striking to observe such a close overlap of their behaviors. To a first approximation both compounds obey the same power law in $(T_i - T)^{1/2}$, even if some small bump seems to appear in the deuterated curve. Transition temperatures are determined by the extrapolation of the curves at zero frequency and within the experimental accuracy (± 1 K) they are compatible with the same 150-K value already obtained by earlier independent studies on hydrogenated compounds [23,29]. Without having the possibility to analyze the very low-frequency behavior like in the hydrogenated crystal, we know from previous inelastic neutron-scattering experiments that the soft mode seems to saturate at about 3 cm^{-1} at a couple of kelvin of T_i [13]. The linewidth evolution of the amplitudon was reported in [22]. Like in the hydrogenated compound, this mode presents an unusually small damping. According to the above paragraph, the inertia increase due to deuteration should also decrease the amplitudon frequency. However, due its low value and the small, calculated variation for external modes and the symmetric phenyl bending, all in the percent range, the difference should be much smaller (0.1 cm^{-1}) than the accuracy of the spectrometer (0.5 cm^{-1}). On the contrary, the chlorophenyl torsions would produce a measurable shift (1 cm^{-1}) if they were the main component of this mode. Since the measured values of the deuterated amplitudon frequencies are at least equal to the hydrogenated ones, it implies that these torsions

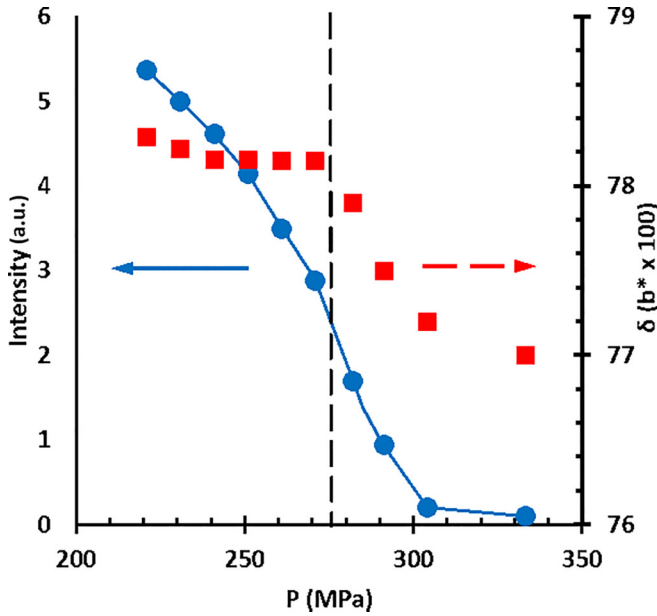


FIG. 7. Coherent neutron-scattering results of BCPS at $T = 50$ K as a function of hydrostatic pressure. In red squares, the incommensurate parameter δ in bis-chlorophenylsulfone, and in blue circles the intensity of diffuse scattering and of the satellite Bragg peak of bis-chlorophenylsulfone measured at $\mathbf{q}_s = \delta \mathbf{b}^*$.

are not involved in the soft mode pattern in agreement with the room-temperature observations.

IV. HYDROSTATIC PRESSURE INVESTIGATIONS

A. Neutron-scattering studies at 50 K

1. Structural features

In order to decrease the soft mode damping, a low-temperature triple-axis neutron study was achieved at 50 K. This value was retained as the lowest one avoiding the solidification of the helium transmitting pressure at the highest studied pressure. The phase transition was determined following the intensity of the satellite Bragg peak, which presents an inflection point. According to the retained notation at ambient pressure, these satellites are located along the vector \mathbf{b}^* of the high-symmetry monoclinic phase $I2/a$ at positions $+/- \mathbf{q}_s = +/- \delta \mathbf{b}^*$. Above the critical pressure transition P_i , they appear as a pretransitional diffuse scattering signaling short-range incommensurate feature within the high-symmetry phase. Measurements were performed at constant temperature as a function of pressure. Figure 7 shows at $T = 50$ K the variation of the parameter of incommensurability δ versus pressure. An abrupt change of slope is located between 270 and 280 MPa. On increasing the pressure, the incommensurate parameter δ decreases. Pretransitional diffuse scattering persists up to 100 MPa above P_i . The determination of the transition pressure comes also from the pressure evolution of the intensity of the diffuse scattering and of the Bragg satellite which presents an inflection point at $P_i = 275 \pm 5$ MPa at 50 K. According to the study performed previously at atmospheric pressure [34], the misfit parameter evolves from $\delta = 0.775$ at $T_i = 150$ K to $\delta = 0.784$ at $T_i = 50$ K and up to $\delta = 0.787$ at 15 K. At

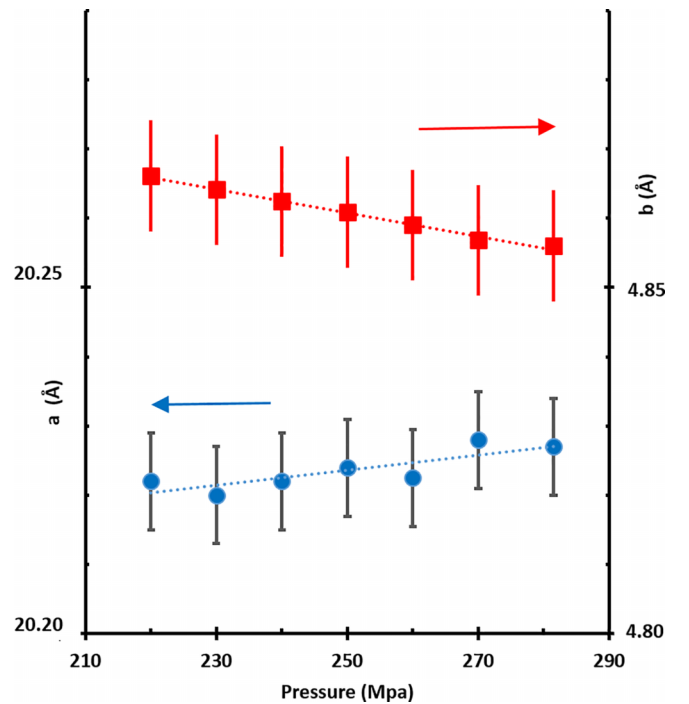


FIG. 8. The parameters \mathbf{a} and \mathbf{b} of the mean monoclinic unit cell $I2/a$ of bis-chlorophenylsulfone vs pressure at $T = 50$ K.

$T = 50$ K, the misfit parameter thus varies quite slowly in the incommensurate phase from $\delta = 0.784$ at atmospheric pressure to $\delta = 0.782$ at $P_i = 275$ MPa. In the high-temperature phase, the intensity maximum of the diffuse scattering tends towards 0.771 at 330 MPa. None of these values are close to any simple rational number.

Supplementary information from the high spatial resolution was obtained during this experiment. This information concerns the evolution of the parameters of the unit cell of the monoclinic $I2/a$ unit cell of bis-chlorophenyl sulfone. On applying pressure from 200 to 280 MPa at 50 K, Fig. 8 shows a slight tendency to increase the parameter \mathbf{a} on increasing pressure within the incommensurate phase. This anomalous negative linear compressibility given by $-1/u(du/dP)$ and the anomalous negative linear expansion at atmospheric pressure, although fundamentally different, are certainly somehow linked. This negative behavior is rather common in monoclinic crystals and is often the result of a hinge due to a soft shearing in the crystal structure [35]. For the parameter \mathbf{b} , a usual decrease is observed in the whole pressure range, which corresponds to a linear compressibility about 40 TPa^{-1} whereas it is negative about -4 TPa^{-1} along \mathbf{a} .

2. Low-frequency dynamics

The 4F1 triple-axis spectrometer provides the unique opportunity to measure the collective critical excitations at various locations in the reciprocal space as a function of pressure. The phase transition remains of displacive regime, and since the transition temperature decreases to zero, this transition is expected to reach the limit of the displacive phase

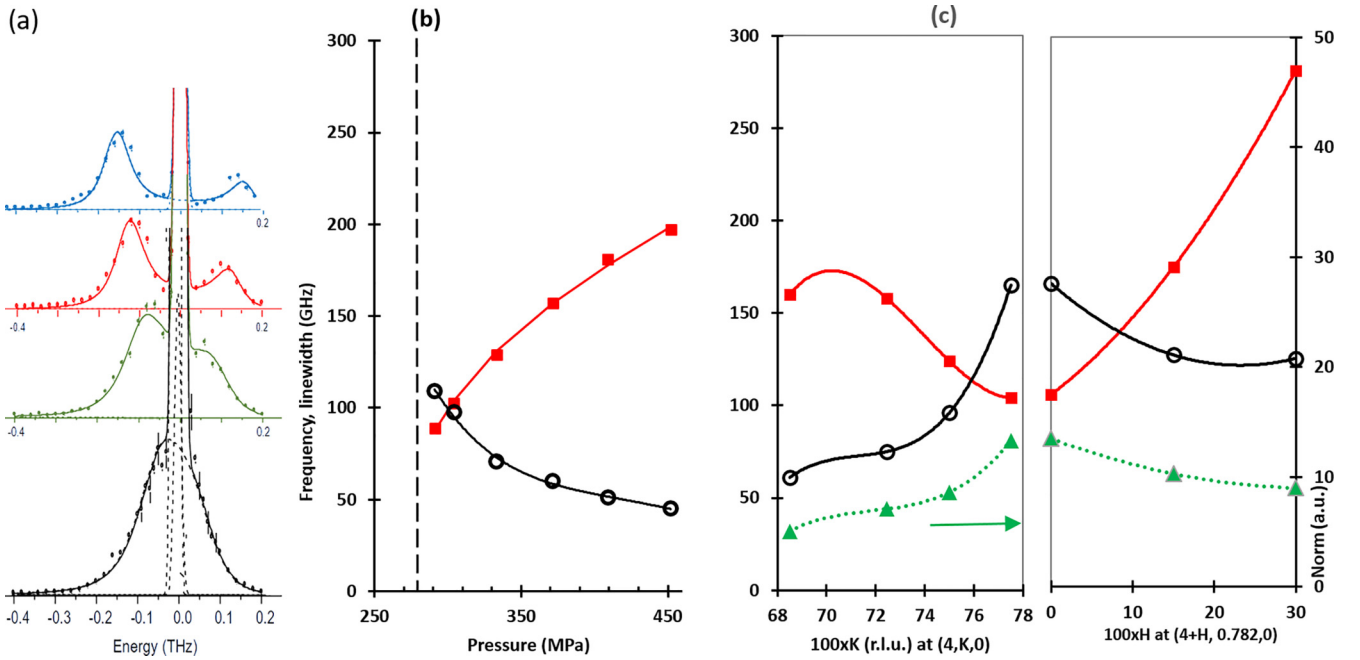


FIG. 9. (a) The inelastic neutron-scattering spectra of deuterated bis-chlorophenylsulfone at $T = 50$ K measured at the minimum of the phonon branch $\mathbf{q}_s = \delta\mathbf{b}^*$, at different pressures from top to bottom: 371, 331, 304, and 292 MPa. (b) Pressure dependence of the frequency (red squares) and of the damping (black circles) of the soft mode measured at \mathbf{q}_s where lines are guides to the eye. (c) Dispersion of the soft phonon branch along the \mathbf{a}^* (Q_h) and the \mathbf{b}^* (Q_k) directions at $P = 292$ MPa with the same symbols for frequency and damping, whereas the norm of this mode relates to green triangles and lines as guides to the eye.

transition [30]. One main feature of this molecular compound is the low damping of the soft mode. At ambient pressure with a phase transition at $T_i = 150$ K, the frequency of the soft mode is $\omega_0 = 240$ GHz at 300 K and its damping $\Gamma = 120$ GHz (4cm^{-1}). Thus, we have here a golden opportunity to decrease this thermal damping. The temperature of $T = 50$ K was retained for the constant pressure study in order to avoid the difficulty associated with the solidification of the helium transmitting pressure at high pressure. The measured coherent neutron-scattering spectra measured at the critical wave vector \mathbf{q}_s are reported in Figs. 9(a) and 9(b). The inelastic spectra are fitted assuming a classical damped oscillator far above the critical transition pressure $P_i = 275$ MPa. At the highest measured pressure, the frequency of the soft mode is $\omega_0 = 200$ GHz and its damping $\Gamma = 45$ GHz as shown in Fig. 9(c). Such a simple description of the inelastic spectrum is valid down to $P = P_i + 25$ MPa, the soft mode remaining underdamped. A more complex feature appears on approaching the transition point. In addition to the soft mode signature, an elastic (nonresolved in energy) contribution must be introduced in the fitting process [dashed line at $P = 292$ MPa in Fig. 9(a)]. Figure 9(b) shows an important increase of the observed inelastic soft mode frequency with an overdamping at P_i which appears as an intrinsic property of this transition. The neutron spectra in the incommensurate phase at 50 K and $P = 200$ MPa clearly exhibit phason and amplitudon modes at the satellite position \mathbf{q}_s [Fig. 10(a)], as expected for incommensurate phases [36]. Deep in the incommensurate phase, both modes are well underdamped and disperse with a shallow minimum at \mathbf{q}_s [Fig. 10(b)].

B. Raman study of the amplitudon evolution and phase diagram.

Using a helium gas pressure, Stokes and anti-Stokes sides of the Raman spectra were limited to the amplitudon frequency range below 20 cm^{-1} . The soft mode frequency squared for the 60-MPa isobar, reveals that the displacive regime of this transition remains under pressure even if the slope and the transition temperature exhibit noticeable variations as shown in Fig. 6. Although isobars allow a direct linear extrapolation of the frequency squared variation of the amplitudon, they require long elapsed times to reach the thermal equilibrium of the massive pressure cell. For this reason, isotherm experiments have been performed on a limited frequency range compatible with optical limitations of the pressurized crystals. An increasing pressure shows at first glance that the incommensurate phase disappears at relatively low pressure.

In Fig. 11, symbols display the measured amplitudon frequency squared on several isotherms. They reveal, first a T_i decrease with a large change of slope and secondly, a noticeable curvature oriented towards the origin. At variance to isotherms, a linear extrapolation to 0 cm^{-1} of the frequency squared leads to erroneous values when the lowest frequencies cannot be reached, whereas the extrapolation to atmospheric pressure would yield to errors as big as 100% on the amplitudon frequency squares. Since these atmospheric quantities are known here from Fig. 6 up to 80 cm^{-2} and above in Ref. [23], a fit including these values should be more realistic. Amplitudon frequency values below 3 cm^{-1} are avoided due to saturation close to the transition [13,22].

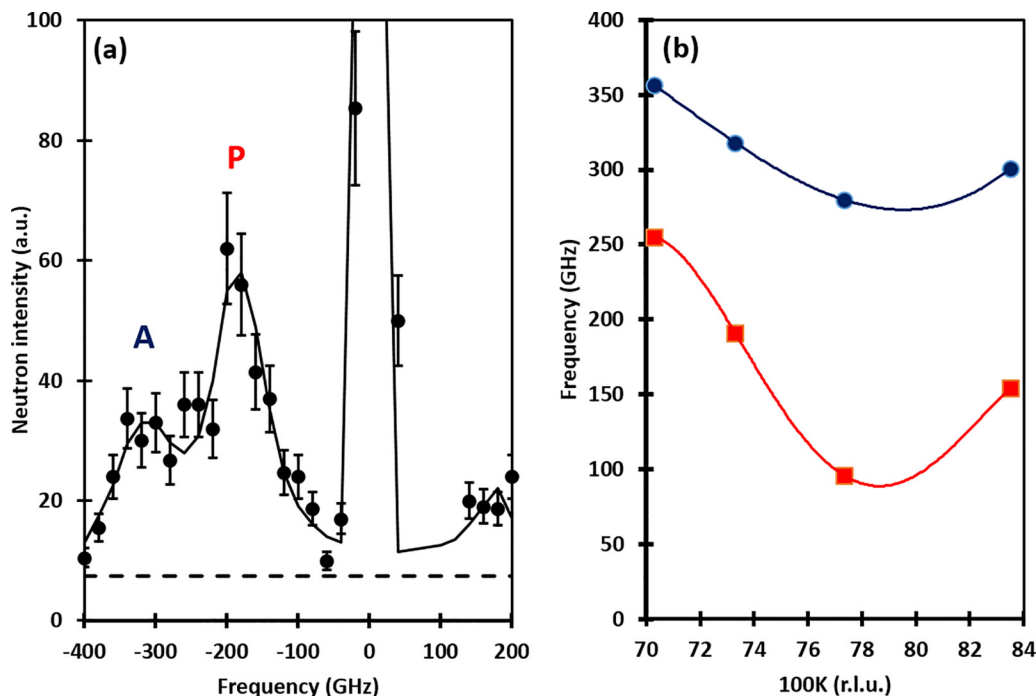


FIG. 10. (a) Phason and amplitudon measured at 50 K, $P = 200$ MPa within the incommensurate phase at the position $(4, 0.733, 0)$; (b) dispersion of the frequencies of the phason and the amplitudon along \mathbf{b}^* around the critical incommensurate vector ($\delta = 0.782$).

Considering that pressure does not significantly modify the amplitudon, one can try to describe the soft mode behavior by a simple temperature effect leading to $\nu_n^2(P) = A_n [T_i(P) - T_n]$, where the index “ n ” is related to the isotherm temperature T_n . Then, the amplitudon frequency square plays

the role of a thermometer with a sensitivity $1/A_n$ varying slightly with temperature. The ten isotherm experiments generate a set of $[T_i(P) - T_n]$ values producing a set of more than 80 $T_i(P)$ values, represented by colored dots in Fig. 12. The alignment of these points in a $T_i(P)$ diagram using an empirical model suggests that this numerical model gives a

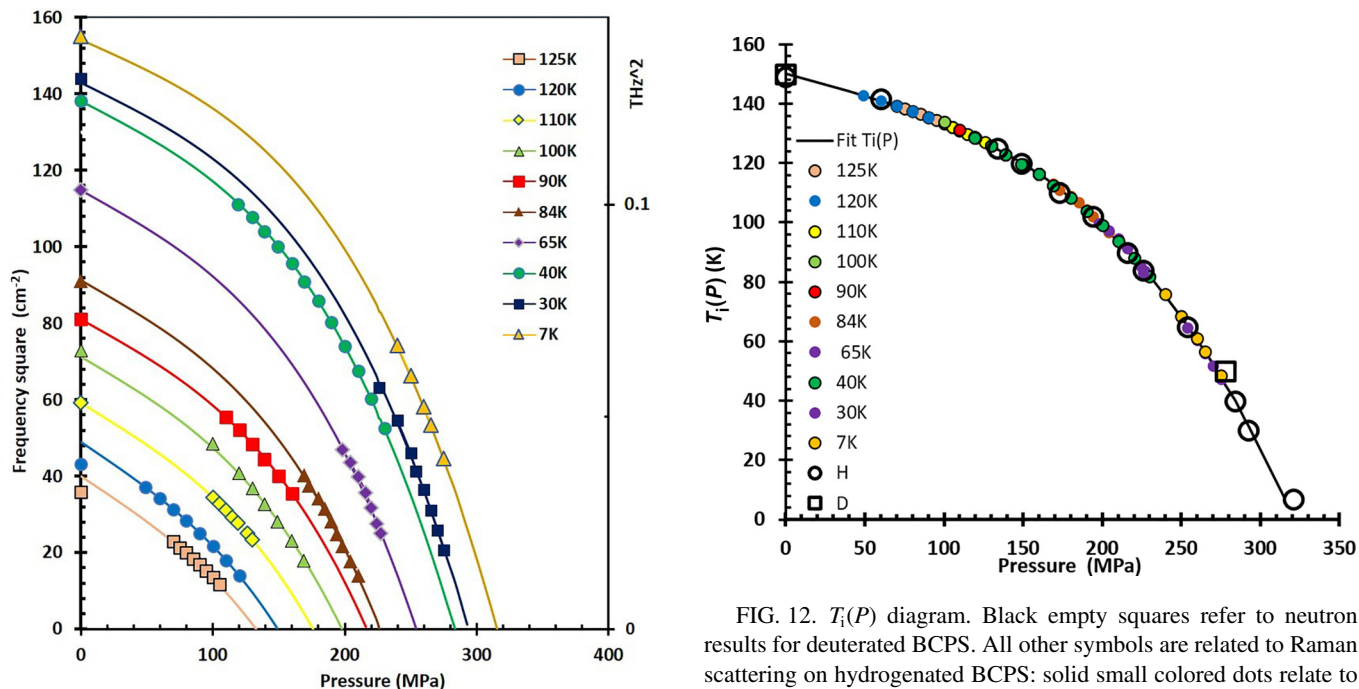


FIG. 11. Amplitudon frequency squared versus pressure from Raman scattering at different isotherms. Symbols refer to measured values whereas lines are obtained with the best fit model.

FIG. 12. $T_i(P)$ diagram. Black empty squares refer to neutron results for deuterated BCPS. All other symbols are related to Raman scattering on hydrogenated BCPS: solid small colored dots relate to each Raman measurement for a given isotherm coded by a color, while larger empty circles correspond to their extrapolated transition pressure value for each isotherm. The pressure errors are never larger than empty symbols below 30 K.

reliable description of the phase diagram. Then, the extrapolated critical pressures $P_i(T_n)$, where the amplitudon frequency should vanish, provide ten additional values represented by black empty circles, called H , in the $T_i(P)$ diagram. Two cases are considered which lead to an equal goodness of fit above 40 K. One is assuming a vertical slope at the lowest temperature with a quartic decrease in pressure leading to $T_i[P(\text{GPa})] = 334.1(P_0 - P)^{1/2} - 360.6(P_0 - P)^2$ with $P_0 = 0.293$ GPa. The other one, almost identical above 40 K, better describes the lowest temperature values obtained below the solidification of helium where the hydrostatic stress state can still be assumed. The best agreement appears to be $T_i[P(\text{GPa})] = 150 - 143.6P - 157P^{3.2}$ where the transition should vanish at about 0.32 GPa. Using this last case, Fig. 11 shows a fit of very good quality describing the evolution of the amplitudon frequency squared for each isotherm in agreement with values at atmospheric pressure. As shown in Fig. 12, each color point corresponds to a Raman frequency measured on isotherms labeled by different colors, whereas black empty circles refer to the extrapolated P_i values using the numerical $T_i(P)$ description for isotherms or directly from the isobars at atmospheric pressure and at 60 MPa. They agree very well with the calculated temperature values at each applied pressure, since only a few points differ by more than a couple of kelvins from the fit. In the case of deuterated crystal, coded by empty black squares in Fig. 12, a very small difference of transition temperature, less than 1 K, could exist at atmospheric pressure. At 50 K, a small pressure shift of 3 MPa equivalent to a temperature shift of 2 K is observed in the diagram. Although these shifts have the same sign, their values are too small to detect a significant effect due to an internal pressure effect generated by deuteration due to the ± 5 MPa error on P_i at 50 K.

V. CONCLUSION

We have used two complementary approaches, isotopic exchange and hydrostatic pressure, to modify the interactions and study their effect on lattice vibrations. We show via deuteration that the internal modes relative to chlorophenyl cycle torsions have frequencies in the upper range of the lattice modes spectrum. This impedes the highest Bg mode above 100 cm^{-1} to play the role of a primary order parameter.

Moreover, the transition temperature reveals a significant difference with the biphenyl behavior where the relative variation of transition temperatures due to isotopic exchange reaches 10% [37] whereas in BCPS it is negligible. From the static point of view, it appears from the neutron-diffraction measurements that the \mathbf{a} lattice parameter of the mean unit cell slightly increases when increasing pressure within the incommensurate phase, indicating a negative compressibility. We show by a detailed study of the anharmonic hard modes that different behaviors vs temperature for the Ag and Bg modes are in relation to the anomalous linear expansion along this \mathbf{a} direction of the crystal lattice. Under pressure, the misfit parameter very slightly decreases in the incommensurate phase remaining at around 0.782, corresponding also to a negative compressibility of the modulation wavelength. This measurement under pressure confirms that there is no tendency for the critical wave vector to approach any commensurable value.

By studying the amplitudon frequency with light scattering under pressure, we reveal the phase diagram of this crystal. The transition temperature of the incommensurate phase goes to zero at about $P = 320$ MPa. There the phase transition is governed by quantum fluctuations and this structural phase transition is in the so-called displacive limit. We conclude that the intermolecular forces increase induced by the pressure increase reduce the anharmonicity of the energy potential associated to the antagonistic forces. Above $P_i = 320$ MPa, this anharmonicity vanishes. We have taken advantage of the decrease of the transition temperature under pressure to study the softening and the dispersion of the critical soft mode at and around the critical wave vector at 50 K by inelastic neutron scattering. Compared to previous ambient pressure studies, the damping of the involved soft phonon modes is significantly reduced in the high-symmetry phase far above the critical pressure value. The increased damping leading to an overdamped feature at $T_i(P = 275 \text{ MPa}) = 50$ K is the signature of an intrinsic complex feature in this inelastic critical response at the transition. Such studies should be pursued when the incommensurate transition temperature T_i approaches 0 K, combining, under pressure, light- and neutron-scattering spectroscopies together with calorimetric and resonance ones in order to understand the critical phase transitions in the displacive limit in the presence of supplementary very low-energy non-Goldstone excitations.

-
- [1] R. Blinc and A. P. Levanyuk, *Incommensurate Phases in Dielectrics* (North-Holland, Amsterdam, 1986), Vols. 1 and 2.
 - [2] H. Z. Cummins, Experimental studies of structurally incommensurate crystal phases, *Phys. Rep.* **185**, 211 (1998).
 - [3] T. Janssen and A. Janner, Aperiodic crystals and superspace concepts, *Acta Crystallogr. B: Struct. Sci., Cryst. Eng. Mater.* **70**, 617 (2014).
 - [4] T. Janssen, G. Chapuis, and M. de Boissieu, *Aperiodic Crystals: From Modulated Phases to Quasicrystals* (Oxford University Press, Oxford, 2007).
 - [5] S. van Smaalen, *Incommensurate Crystallography* (Oxford University Press, Oxford, 2007).
 - [6] C. Benkert, V. Heine, and E. H. Simmons, Absence of lock-in transition in some incommensurate materials, *Europhys. Lett.* **3**, 833 (1987).
 - [7] D. J. Pusiol, A. E. Wolfenson, and A. H. Brunetti, A possible incommensurate system, *Phys. Rev. B* **40**, 2523 (1989).
 - [8] H. Kasano, T. Toshiba, H. Kasatami, and H. Tekauchi, Incommensurate phase transition in 4,4'-dichlorodiphenyl sulfone, *J. Phys. Soc. Jpn.* **59**, 408 (1990).
 - [9] R. E. de Souza, M. Engelsberg, and D. J. Pusiol, Proton spin-lattice relaxation and phason dynamics in dichlorobiphenylsulfone, *Phys. Rev. Lett.* **66**, 1505 (1991).

- [10] J. Etrillard, J. Even, M. Sougoti, P. Launois, S. Longeville, and B. Toudic, Elastic neutron scattering study of high order satellites in the incommensurate phase of bis(4-chlorophenyl)sulfone, *Sol. State Comm.* **87**, 47 (1993).
- [11] F. J. Zuniga, J. M. Perez-Mato, and T. Breczewski, Structure of the incommensurate phase of 4,4'-dichlorobiphenyl sulfone at 90 K, *Acta Crystallogr. B: Struct. Sci., Cryst. Eng. Mater.* **49**, 1060 (1993).
- [12] R. Blinc, T. Apih, J. Dolinšek, U. Mikac, D. C. Ailion, and P.-H. Chan, ^{35}Cl spin-lattice relaxation in incommensurate bis(4-chlorophenyl)sulfone, *Phys. Rev. B* **51**, 1354 (1995).
- [13] J. Ollivier, J. Etrillard, B. Toudic, C. Ecolivet, P. Bourges, and A. P. Levanyuk, Direct observation of a phason gap in an incommensurate molecular compound, *Phys. Rev. Lett.* **81**, 3667 (1998).
- [14] C. Barta, A. A. Kaplyanski, V. V. Kulakov, and Y. B. Markov, Raman scattering spectra and structural phase transitions in the improper ferroelastics Hg_2Cl_2 and Hg_2Br_2 , *JETP Lett.* **21**, 121 (1975).
- [15] D. M. Hanson, Direct observation of a soft phonon associated with a structural phase transition in a molecular crystal, *J. Chem. Phys.* **63**, 5046 (1975); A. Girard, Y. Delugeard, and C. Ecolivet, Further Raman investigation of the chloranil soft mode using an iodine cell, *J. Phys. C: Solid State Phys.* **20**, 601 (1987).
- [16] J. Etrillard, J. C. Lasjaunias, K. Biljakovic, B. Toudic, and G. Coddens, Excess low temperature specific heat and related phonon density of states in a modulated incommensurate dielectric, *Phys. Rev. Lett.* **76**, 2334 (1996).
- [17] H. Ochoa and R. M. Fernandes, Extended linear-in- T resistivity due to electron-phonon scattering in moiré superlattices, *Phys. Rev. B* **108**, 075168 (2023).
- [18] A. P. Levanyuk, S. A. Minyukov, J. Etrillard, and B. Toudic, Low-frequency phonon dynamics and spin-lattice relaxation time in the incommensurate phase at low temperatures, *Phys. Rev. B* **56**, 8734 (1997).
- [19] A. Taye, D. Michel, and J. Petersson, Phason and amplitude dynamics in the incommensurate phase of bis(4-chlorophenyl)sulphone, *Phys. Rev. B* **69**, 224206 (2004).
- [20] S. M. Shapiro, J. D. Axe, G. Shirane, and T. Riste, Critical neutron scattering in SrTiO_3 and KMnF_3 , *Phys. Rev. B* **6**, 4332 (1972).
- [21] P. A. Fleury and K. B. Lyons, Central-peak dynamics at the ferroelectric transition in lead germanate, *Phys. Rev. Lett.* **37**, 1088 (1976).
- [22] C. Ecolivet, M. Sougoti, Y. Delugeard, and A. Girard, High resolution Raman study of the soft mode in the incommensurate bis(4-chlorophenyl)sulfone, *J. Phys. (France)* **4**, 1451 (1994).
- [23] K. Ishii, H. Nakayama, T. Sakato, and H. Kano, Raman and birefringence studies on the incommensurate phase transition of bis(4-chlorophenyl)sulfone crystal, *J. Phys. Soc. Jpn.* **61**, 2317 (1992).
- [24] H. Cailleau, in *Incommensurate Phases in Dielectrics: Parts 1 and 2, Modern Problems in Condensed Matter Sciences*, edited by R. Blinc and A. P. Levanyuk (North-Holland, Amsterdam, 1986), Vol. 14.
- [25] K. Saito, K. Kikuchi, and I. Ikemoto, Incommensurate crystal-instability and a role of internal degrees of freedom in bis(4-chlorophenyl) sulfone molecules, *Solid State Commun.* **81**, 241 (1992).
- [26] A. Criado, Lattice dynamics, Raman spectra and soft mode in 4-4'-dichlorodiphenylsulfone, *J. Phys. Soc. Jpn.* **64**, 2470 (1995).
- [27] J. Schneider, H. C. Panepucci, M. C. dos Santos, C. A. Meriles, and L. A. O. Nunes, Lattice dynamics and structural instabilities in biphenyl sulfone derivatives, *J. Phys. Soc. Jpn.* **68**, 493 (1999).
- [28] Y. Pan and G. Chapuis, Molecular dynamics investigations of modulated phases in organic materials, *Acta Crystallogr. A* **61**, 19 (2005).
- [29] J. Schneider, L. A. O. Nunes, and H. Panepucci, Structural instabilities in bis(4-chlorophenyl)sulfone derivatives studied by Raman spectroscopy and deuteron NMR, *Phys. Rev. B* **64**, 094103 (2001).
- [30] R. Opperman and H. Thomas, Critical behaviour at the displacive limit of structural phase transitions, *Z. Phys. B* **22**, 387 (1975).
- [31] A. N. Wynchell, *Optical Properties of Organic Crystals*, 2nd ed. (University of Wisconsin Press, Madison, 1954).
- [32] A. Girard, Y. Delugeard, L. Pichon, and B. Toudic, Structural phase transition in p-quaterphenyl: A Raman study of the influence of temperature and pressure, *J. Phys. I: France* **2**, 1833 (1992).
- [33] H. Poulet and R. M. Pick, Light scattering in displacive incommensurate structures: A Landau theory approach, *J. Phys. C* **14**, 2675 (1981).
- [34] J. Ollivier, J. Etrillard, M. Sougoti, B. Toudic, C. Ecolivet, and P. Bourges, Structural and dynamical aspects of the incommensurate molecular system Bis(4-chlorophenyl) sulfone, *Ferroelectrics* **183**, 283 (1996).
- [35] A. B. Cairn and A. L. Goodwin, Negative linear compressibility, *Phys. Chem. Chem. Phys.* **17**, 20449 (2015).
- [36] J. D. Axe, M. Iizumi, and G. Shirane, Lattice dynamics of commensurate and incommensurate K_2SeO_4 , *Phys. Rev. B* **22**, 3408 (1980).
- [37] K. Saito, T. Atake, and H. Chihara, Calorimetric studies of successive phase transitions in crystalline biphenyl- d_{10} , *J. Chem. Thermodyn.* **19**, 633 (1987).